Testing the efficacy of the glacial buzzsaw: insights from the Sredinny Mountains, Kamchatka

Iestyn D. Barr[a,*], **Matteo Spagnolo**[b,l]

[a]*School of Geography, Archaeology and Palaeoecology, Queen's University Belfast, BT7 1NN, Belfast, UK.*

[b]*School of Geosciences, University of Aberdeen, Elphinstone Road, AB243UF, Aberdeen, UK.*

*Corresponding author. Tel.: +44 (0)2890 975146; E-mail: i.barr@qub.ac.uk.
[l]Tel.: +44 (0)1224 273034; Fax: +44 (0)1224 278585; E-mail: m.spagnolo@abdn.ac.uk.

This is an author produced version of a paper published in **Geomorphology**

Published paper:

Barr. I.D., Spagnolo, M. (2014) Testing the efficacy of the glacial buzzsaw: insights from the Sredinny Mountains, Kamchatka, Geomorphology 206, 230-238. doi: 10.1016/j.geomorph.2013.09.026

http://www.sciencedirect.com/science/article/pii/S0169555X13005084

Testing the efficacy of the glacial buzzsaw: insights from the Sredinny Mountains, Kamchatka

Iestyn D. Barr[a,*], **Matteo Spagnolo**[b,l]

[a]*School of Geography, Archaeology and Palaeoecology, Queen's University Belfast, BT7 1NN, Belfast, UK.*

[b]*School of Geosciences, University of Aberdeen, Elphinstone Road, AB243UF, Aberdeen, UK.*

*Corresponding author. Tel.: +44 (0)2890 975146; E-mail: i.barr@qub.ac.uk.
[l]Tel.: +44 (0)1224 273034; Fax: +44 (0)1224 278585; E-mail: m.spagnolo@abdn.ac.uk.

Abstract

Peak altitudes, hypsometry, geology, and former equilibrium-line altitudes (ELAs) are analyzed across the Sredinny Mountains (Kamchatka). Overall, evidence is found to suggest that the glacial buzzsaw has operated to shape the topography of this mountain range, but the strength of this signature is not spatially uniform. In the southern sector of the mountains, we see evidence that an efficient glacial buzzsaw has acted to impose constraints upon topography, limiting peak altitudes, and concentrating land-surface area (hypsometric maxima) close to palaeo-ELAs. By contrast, in the northern sector of the mountains, a number of peaks rise high above the surrounding topography, and land-surface area is concentrated well below palaeo-ELAs. This deviation from a classic 'buzzsaw signature', in the northern sector of the mountains, is considered to reflect volcanic construction during the Quaternary, resulting in a series of high altitude peaks, combined with the action of dynamic glaciers, acting to skew basin topography toward low altitudes, well below palaeo-ELAs. These glaciers are considered to have been particularly dynamic because of their off-shore termination, their proximity to moisture-bearing air masses from the North Pacific, and because accumulation was supplemented by snow and ice avalanching from local high altitude peaks. Overall, the data suggest that the buzzsaw remains a valid mechanism to generally explain landscape evolution in mountain regions, but its signature is significantly weakened in mountain basins that experience both volcanic construction and climatic conditions favouring dynamic glaciation.

Keywords: glacial buzzsaw; glacial erosion; landscape evolution; glacial geomorphology; hypsometry; topography

1. Introduction

Mountain chains play an important role in governing global and regional climate patterns by acting as orographic barriers to atmospheric flow (e.g., Bookhagen and Strecker, 2008; Galewsky, 2009). Therefore investigating the processes and timescales responsible for their development is important. In general, topographic development is governed by the interaction of uplift, largely driven by tectonic processes, and denudation by various forms of weathering, erosion, and mass movement (e.g., Small and Anderson, 1995; Brocklehurst and Whipple, 2002). Across much of the globe, denudation is generally governed by fluvial and slope processes, yet in many mountainous and high to mid-latitude environments, glacial processes become dominant and represent the main players in shaping large-scale topography (see Egholm et al., 2009). The role of glaciers as denudational agents is largely governed by subglacial erosion, through a combination of abrasion, plucking, and subglacial fluvial drainage (see Krabbendam and Glasser, 2011; Cowton et al., 2012) (though associated periglacial processes also contribute). The efficacy of these mechanisms is a function of ice velocity, thickness, subglacial water pressure, and bedrock properties; but in general terms, the intensity of subglacial erosion is greatest where total ice-flux and subglacial sliding velocity are maximized (see Harbor et al., 1988; Humphrey and Raymond, 1994; MacGregor et al., 2000; Tomkin and Braun, 2002; Amundson and Iverson, 2006). For most glaciers, this area where erosion is maximized is considered to coincide with the equilibrium-line altitude (ELA) where net annual accumulation and ablation are equal (Boulton, 1996; Hallet et al., 1996; MacGregor et al., 2000; Anderson et al., 2006). The position of the ELA is governed by local factors such as topographic shading and avalanching, but at a regional scale is largely determined by climate (air temperatures and snowfall) (e.g., Ohmura et al., 1992). With glacial erosion maximized at the ELA, topography above this altitude progressively steepens, as valley sides and cirque headwalls are undercut and become prone to periglacially induced rock detachments and slope failures (Oskin and Burbank, 2005; Sanders et al., 2012). These processes act to enlarge valleys above the ELA and limit the altitudes attained by mountain peaks (Oskin and Burbank, 2005; Mitchell and Montgomery, 2006; Sanders et al., 2012). Below the ELA, erosion is limited by reduced ice flux and sliding velocity and by a system generally prone to being engulfed by glacial sediments that inhibit post-glacial fluvial erosion (e.g., Whipple et al., 1999). These combined processes of erosion and deposition above, at, and below the ELA result in the classic ‘glacial buzzsaw’ landscape, characterized by a concentration of eroded topography close to palaeo-ELAs and in a clear correlation between peak altitudes and palaeo-ELAs (Brozović et al., 1997; Montgomery et al., 2001; Brocklehurst and Whipple, 2002; Mitchell and Montgomery, 2006; Foster et al., 2008; Egholm et al., 2009; Pedersen et al., 2010). Though such a signature can be found in many mountain ranges globally (Porter, 1964; Richmond, 1965; Brozović et al., 1997), the efficacy of the buzzsaw effectively relies upon a balance between glacial and tectonic forces—and clearly, many exceptions are possible (e.g., Brocklehurst and Whipple, 2007; Foster et al., 2010; Pedersen et al., 2010; Ward et al., 2012). For example, climatic factors can enhance or inhibit the formation and erosional power of glaciers (e.g., Thomson et al., 2010), as can factors related to bedrock lithology and structure. This paper considers the role of geological and climatic forces in mitigating the glacial buzzsaw within the Sredinny Mountains, Kamchatka.

2. Previous investigations

A number of studies have considered the role of the glacial buzzsaw in regulating the topography of mountain massifs around the world. Brozović et al. (1997), investigating actively deforming mountains in the NW Himalaya, were the first to identify and outline the

landscape-signature of the glacial buzzsaw. Subsequent investigations demonstrated the prevalence of this signature in the mountains of North America (Spotila et al., 2004; Mitchell and Montgomery, 2006; Foster et al., 2008, 2010; Ward et al., 2012), South America (Thomson et al., 2010), New Zealand (Brocklehurst and Whipple, 2007), Switzerland (Anders et al., 2010), and at a global scale (Egholm et al., 2009; Pedersen et al., 2010). Deviations from the 'classic' buzzsaw signature have been linked to tectonics and bedrock strength (see Foster et al., 2008, 2010; Thomson et al., 2010; Ward et al., 2012) and used to infer the former presence of minimally erosive glaciers (Thomson et al., 2010).

3. Study area

The geographical focus of this investigation is upon the Sredinny Mountains, which represent the central topographic divide of the Kamchatka Peninsula (see Fig. 1). The mountain range is ~ 800 km long, up to ~ 100 km wide, and constitutes a series of separate ridges and volcanic plateaus, with peak altitudes typically found between 1500 m above sea level (asl) and 2000 m (asl), reaching a maximum altitude of 3621 m (asl). The mountains are geologically very young and have undergone uplift and deformation during the past 70 Ma or more (Fedotov et al., 1988; Hourigan et al., 2004). The region's generalised lithology is presented in Fig. 1A (based upon Persits et al., 1997; Avdeiko et al., 2007). In total, nine units are distinguished, with ~ 5% of the area comprising Quaternary unconsolidated deposits; ~ 8% comprising Paleocene–Miocene deposits ; ~ 32% comprising Quaternary volcanic complexes ; ~ 30% comprising Miocene–Pliocene volcanic complexes; ~ 2% comprising Eocene volcanic complexes ; ~ 3% comprising collision granitoids; ~ 9% comprising upper Cretaceous and Paleocene volcanic and volcanic-terrigenous deposits; ~ 3% comprising Cretaceous terrigenous deposits; and ~ 8% of the area comprising metamorphic complexes. At present, the range is occupied by 72 extinct and two active volcanoes (Avdeiko et al., 2007), some of which are characterised by considerable Quaternary activity (see Table 2). Direct estimates of Quaternary rock uplift rates are not available, but exhumation rates of between 0.18 and 0.67 mm y^{-1} have been obtained for a single site upon the SE slopes of the range (Hourigan et al., 2004). These estimates are based upon fission-track ages and thermochronology and could be used as a proxy for uplift rates from the late Oligocene to present. However, a point source uplift rate is unrepresentative of the entire region, and variability in uplift rate across the mountains is likely. The Sredinny are currently occupied by a number of small cirque-type glaciers, and evidence suggests that, during the past 140 ka, the mountains were entirely ice covered on at least two separate occasions, with glaciers extending off-shore and terminating in the Sea of Okhotsk and the North Pacific (see Bigg et al., 2008; Nürnberg et al., 2011; Barr and Clark, 2012a,b), though the duration and timing of these events remains uncertain (see Bigg et al., 2008; Barr and Clark, 2012b). During the global Last Glacial Maximum (gLGM; ~ 21 ka) specifically, the region was occupied by an ice field (~ 57,363 km^2) that covered ~ 92% of the mountain range (Barr and Clark, 2011) (see Fig. 1B). This, alongside other geomorphological evidence of glacial erosion and deposition (Barr and Clark, 2011, 2012a,b; Barr and Spagnolo, 2013), indicates that a glaciated landscape dominates most drainage basins of the Sredinny Range. The drainage basins analyzed within the present study cover the entire mountain chain (~ 72,500 km^2) and extend over a latitudinal range of ~ 8° (see Fig. 1).

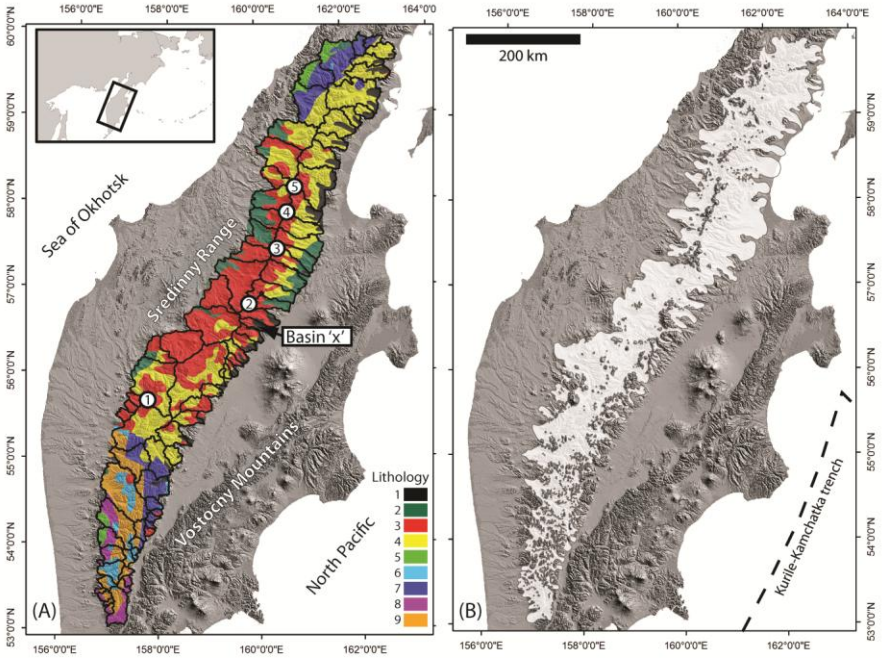

Fig. 1. Map of the Kamchatka Peninsula, focusing upon the Sredinny Mountain Range. (A) Drainage basins (N = 80) analyzed in the present study (outlined in black) and generalised lithology (based upon Persits et al., 1997; Avdeiko et al., 2007). Geological units are (1) Quaternary unconsolidated deposits; (2) Paleocene–Miocene deposits; (3) Quaternary volcanic complexes; (4) Miocene–Pliocene volcanic complexes; (5) Eocene volcanic complexes; (6) collision granitoids; (7) upper Cretaceous and Paleocene volcanic and volcanic-terrigenous deposits; (8) Cretaceous terrigenous deposits; (9) Metamorphic complexes. Numbered peaks are those extending > 500 m above regional trends in peak altitude (peak details are provided in Table 2). The hypsometric attributes of basin 'x' are presented in Fig. 3. (B) The extent of glaciation in the Sredinny Mountains during the global Last Glacial Maximum (according to Barr and Clark, 2011).

4. Methods

In order to consider controls upon the overall morphometry of the Sredinny Mountains, topographic and palaeoglacial attributes were analyzed across the range. Attributes were calculated for the 80 principal drainage basins (catchments) within the mountains. Basins were delineated in ArcGIS from an ~ 30-m resolution digital elevation model (ASTER GDEM), and each was defined as a group of cells related by their flow pathways to an outlet at the mountain range front (see Fig. 2A). The downstream limit of each basin was located at the junction with a lowland river (i.e., a river not directly emanating from the Sredinny Mountains). Comparison between attributes was made at a basin scale, whilst regional variations were considered by plotting transects and producing interpolated (kriged) surfaces.

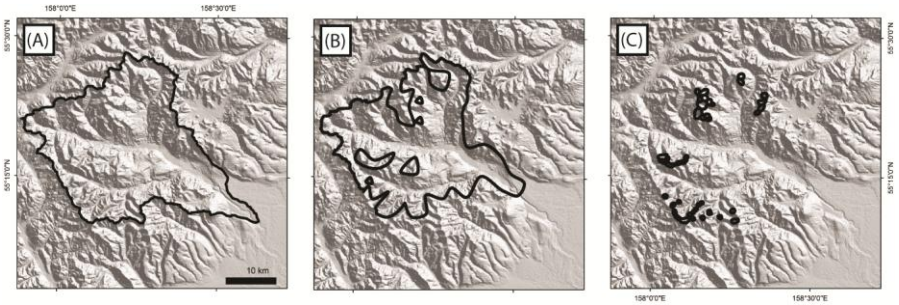

Fig. 2. Example (A) drainage basin; (B) reconstructed gLGM ice extent (according to Barr and Clark, 2011); and (C) cirque distribution (N = 43), in the SE sector of the Sredinny Mountains. Here, the drainage basin is 825 km^2, gLGM ice extent covers 603 km^2, and the cirques cover a total area of 33 km^2.

4.1. Topographic attributes

Topographic attributes were analyzed in ArcGIS, and derived from the ASTER GDEM. For each drainage basin, minimum ($Alt_{(min)}$), mean ($Alt_{(mean)}$), and maximum ($Alt_{(peak)}$) altitudes were extracted directly from the DEM. Hypsometric curves were plotted, (see Fig. 3A) and hypsometric integrals (HI) calculated for each basin using the CalHypso GIS extension of Pérez-Peña et al. (2009). The HI reflects the area of the region under the hypsometric curve (see Fig. 3A) (Strahler, 1952) and, being dimensionless, can be used to compare between basins, irrespective of scale (see Walcott and Summerfield, 2008; Cheng at al., 2012). Other hypsometric attributes were calculated by plotting normalized hypsometric frequency distributions for each drainage basin (see Fig. 3B) (see Foster et al., 2008). Each hypsometric frequency distribution comprised 40 altitudinal bins (following the method employed by Egholm et al., 2009), and hypsometric maxima (*Hmax*) were recorded where an altitude bin had greater area than its four closest neighbours (see Fig. 3B). In basins with multiple hypsometric maxima, all were recorded; but the single most prominent ($Hmax_{(single)}$) is considered here (see Fig. 3B).

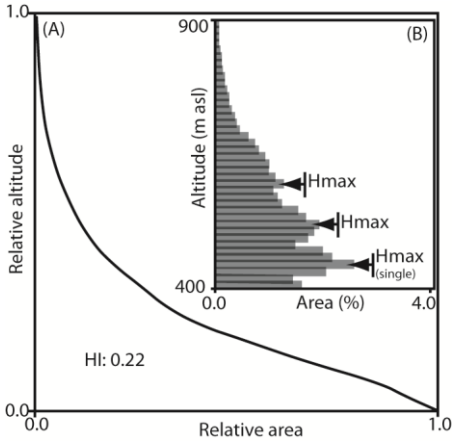

Fig. 3. Hypsometric properties of basin 'x' (see Fig 1A for basin location) to the east of the Sredinny Mountains. (A) Hypsometric curve. HI is the hypsometric integral and reflects the area of the region under the curve. (B) Hypsometric distribution. Hypsometric maxima (*Hmax*) are highlighted (where a bin has more area than its four neighbours). $Hmax_{(single)}$ is the single most prominent hypsometric maximum within the basin.

4.2. Palaeoglacial attributes

For each drainage basin, a number of palaeoglacial attributes were considered, some relating specifically to conditions at the gLGM, others lacking chronological control. Attributes relating to conditions at the gLGM were derived from the ice-field reconstruction of Barr and Clark (2011) (see Fig. 1B). This reconstruction was used to calculate gLGM ELA for each drainage basin (see example in Fig. 2B) using the balance ratio method (BR), with a BR of 1.8 (see Benn and Gemmell, 1997). Mean cirque floor altitude ($cirq_{(alt)}$) was calculated from a data set of 2858 Sredinny cirques presented by Barr and Spagnolo (2013) (see examples in Fig. 2C). Regional $Cirq_{(alt)}$ has been used by previous investigators as an indicator of mean Quaternary equilibrium-line altitude (ELA), based upon the assumption that cirques occupy an intermediate position between gLGM ELAs and modern snowline altitudes (see Porter, 1989; Mitchell and Montgomery, 2006; Foster et al., 2008).

5. Results

Statistics for drainage basins analyzed within the present study are presented in Table 1, and attributes are considered in the sections that follow.

5.1. Topography

The Sredinny Mountains extend from sea level to 3621 m (asl). Generally, peak altitudes are highest in the central sector of the range and decrease toward the north and south. These trends are depicted in Fig. 4 where latitudinal variations in peak altitudes are shown, and a best-fit quadratic regression line is applied to these maximum elevations. From these data (Fig. 4) we see that a number of peaks rise conspicuously above the maximum altitude regression line, especially in the northern sector, sometimes by as much as 1769 m. Peaks extending more than 500 m above the regression line are labelled in Fig. 4 and detailed in Table 2.

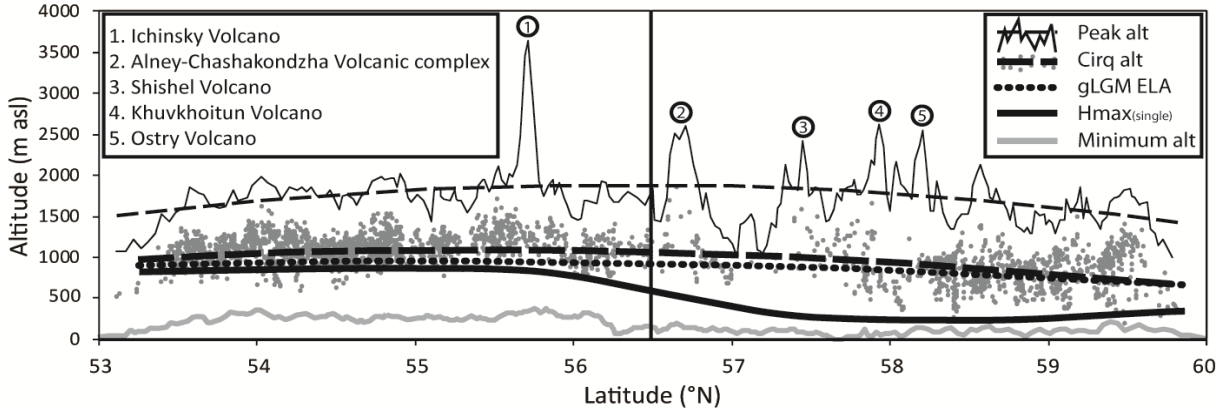

Fig. 4. Swath topographic profile from south to north (53-60° N.) along the Sredinny Mountains. Showing peak altitudes; a best-fit quadratic regression line fitted to these maximum elevations; cirque-floor altitudes (grey dots); a best-fit quadratic regression line fitted to these cirque floor altitudes; a best-fit quadratic regression line fitted to the gLGM ELA data; a best-fit quadratic regression line fitted to the $Hmax_{(single)}$ data; and minimum altitudes (grey line). The solid vertical line marks the approximate boundary between the southern (below 56.5° N.) and northern sector (above 56.5° N.). Numbered peaks are those extending > 500 m above the peak altitude regression line and are detailed in Table 2.

5.2. Hypsometry

Interregional variations in hypsometry are evident across the Sredinny Mountains. Variability in HI and $Hmax_{(single)}$ is shown in Fig. 5 (A and B, respectively), where interpolated values are depicted. From these Figs. (5A and 5B) we see correspondence between attributes, with HI and $Hmax_{(single)}$ attaining highest values towards the southern sector of the range (below ~ 56.5° N.) and lowest values toward the northern sector (above ~ 56.5° N.). Latitudinal (rather than basin scale) variability in $Hmax_{(single)}$ is shown in Fig. 4 and, again, demonstrates that values are higher in the southern sector and generally decrease toward the north.

5.3. Palaeo-ELA

Palaeo-ELAs in the Sredinny Mountains are reflected in $cirq_{(alt)}$ and gLGM ELA. These attributes are positively correlated (R = 0.65, see Table 3) and show comparable trends along the range: with highest values generally found in the southern sector of the range, and lowest values found toward the northern sector (see Figs. 4, 5C-D). The $Cirq_{(alt)}$ and gLGM ELA appear to vary in accord with hypsometric attributes (see Fig. 5A-D), and this is reflected in the positive correlation between these attributes ($0.31 < R < 0.66$, see Table 3). Despite this general correspondence, we see that in the southern sector, peaks in landscape hypsometry ($Hmax_{(single)}$) occur close to $cirq_{(alt)}$ and gLGM ELA regression lines (see Fig. 4); but in the northern sector, peaks in hypsometry occur below these altitudes (see Fig. 4) (a relationship discussed in section 6.2.1).

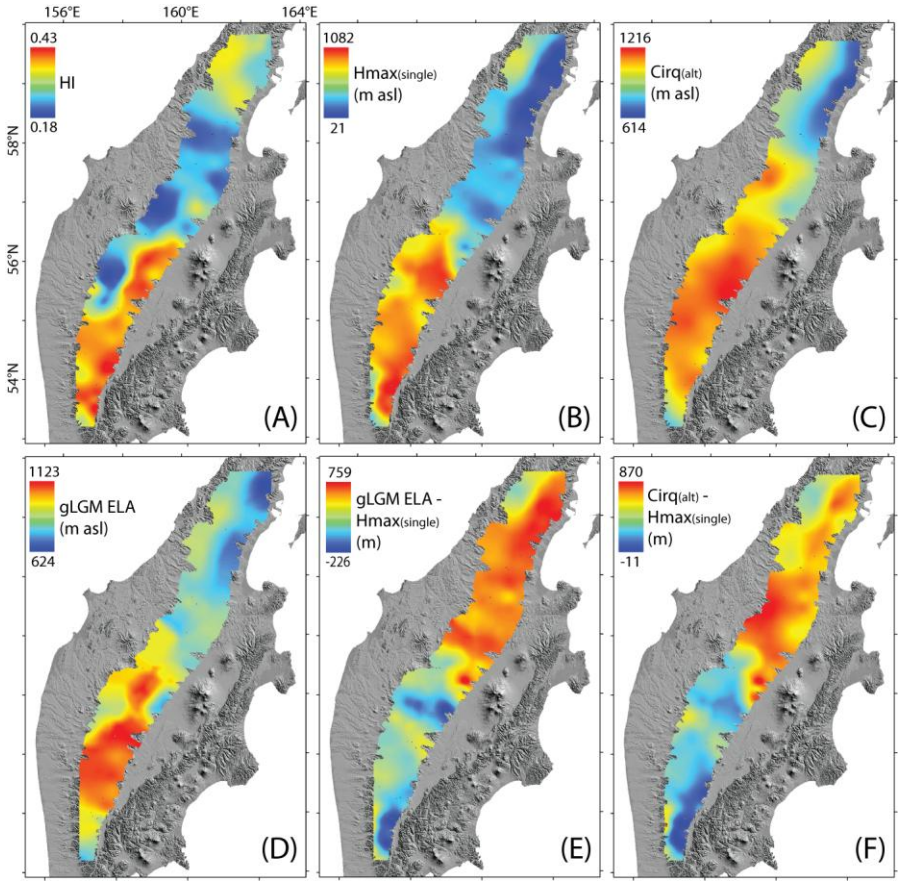

Fig. 5. Basin-scale variability in various attributes across the Sredinny Mountains. (A) Hypsometric integrals (HI). (B) The single most prominent hypsometric maximum within individual basins ($Hmax_{(single)}$). (C) Cirque floor altitudes ($cirq_{(alt)}$). (D) gLGM ELA. (E) 'gLGM ELA - $Hmax_{(single)}$'. (F) '$cirq_{(alt)}$ - $Hmax_{(single)}$'. Figs. reflect interpolated surfaces derived through kriging.

6. Discussion

The topography of the Sredinny Mountains appears to demonstrate significant spatial variability, and this likely reflects a complex combination of tectonic, glacial, fluvial, and other processes. Here, this variability is discussed with specific reference to the glacial buzzsaw.

6.1. Do the Sredinny Mountains preserve a record of the glacial buzzsaw?

The buzzsaw hypothesis states that glacial erosion acts to limit mountain topography, and therefore results in a correlation between peak altitudes and palaeo-ELAs (Brozović et al., 1997; Montgomery et al., 2001; Brocklehurst and Whipple, 2002; Mitchell and Montgomery, 2006; Foster et al., 2008; Egholm et al., 2009; Pedersen et al., 2010). In the Sredinny Mountains, we see a correspondence between peak altitudes and palaeo-ELAs as, when considered for each of the 80 drainage basins, $Alt_{(peak)}$ is positively correlated with both $cirq_{(alt)}$ and gLGM ELA, although the correlation is not exceptionally strong (R = 0.41, and R = 0.27, respectively, see Table 3). When best-fit quadratic regression lines are considered, we see that $Alt_{(peak)}$ tracks $cirq_{(alt)}$ and gLGM ELA (see Fig. 4); with the regression line for peak altitudes found on average 747 and 849 m above the $cirq_{(alt)}$ and gLGM ELA regression lines, respectively. We also see evidence that hypsometric attributes and palaeo-ELAs are related (as predicted by the buzzsaw hypothesis). For example, $Hmax_{(single)}$ is strongly correlated with $cirq_{(alt)}$ and gLGM ELA (R = 0.66 and R = 0.63, respectively, see Table 3), and spatial trends in these attributes are comparable (see Fig. 5B-D). Similarly, HI is correlated with $cirq_{(alt)}$ and gLGM ELA, but to a lesser degree (R = 0.31 and 0.40, respectively, see Table 3); and

again, we see some correspondence between spatial trends in these attributes (see Fig. 5A and 5C-D). Thus, key indicators would appear to suggest the operation of a buzzsaw, with glacial erosion effectively limiting the growth of the Sredinny Mountains.

A crucial aspect of the glacial buzzsaw is that it represents a balance between constructional (e.g., uplift) and destructional (e.g., glacial erosion) forces, the latter effectively being an expression of climatic forcing over landscape evolution. Despite evidence that overall this balance has been in operation in the Sredinny Mountains, the study of both hypsometric peaks and non averaged peak altitudes reveal that the geographical distribution of the glacial buzzsaw signature is not uniform, thus suggesting situations where one of the two forces has prevailed. In agreement with the predictions of the glacial buzzsaw theory, the southern sector of the Sredinny Mountains (< ~ 56.5° N.) shows hypsometric peaks ($Hmax_{(single)}$) close to palaeo-ELAs (see Fig. 4) and, with the exception of Ichinsky Volcano, restricted peak altitudes (see Fig. 4). However, in the northern sector (> ~ 56.5° N.), the efficacy of the glacial buzzsaw is questioned by the fact that (i) hypsometric peaks are found below palaeo-ELAs (see Fig. 4), and (ii) a series of exceptionally high peaks rise conspicuously above the surrounding topography (see Fig. 4). Fact (i) is indicative of a situation where erosional (glacial) processes are prevailing over topographic construction, and fact (ii) suggests localized spots where the opposite is true, with topographic construction outpacing erosion; both are discussed below.

6.2. Where dynamic glaciers prevail

Because glacial erosion is maximised at the ELA and because land surface becomes concentrated at this altitude, one of the key characteristics typically used as evidence of the buzzsaw is a correspondence between hypsometric peaks (*Hmax*) and palaeo-ELAs (see Brozović et al., 1997; Montgomery et al., 2001; Brocklehurst and Whipple, 2002; Mitchell and Montgomery, 2006; Foster et al., 2008; Egholm et al., 2009). In the northern sector of the Sredinny Mountains, this relationship is not apparent because peaks in landscape hypsometry ($Hmax_{(single)}$) occur well below palaeo-ELAs (see Fig. 4). The relationship between hypsometric maxima and palaeo-ELAs has been used previously (e.g., Brocklehurst and Whipple, 2002, 2004; Foster et al., 2008) to infer the action of the glacial buzzsaw, as linked to the 'degree' of former glaciation in a region. In particular, this idea is used to compare regions that were 'partially' and 'fully' ice-covered during former periods of glaciation, based upon the assumption that (i) coincidence between peaks in landscape hypsometry and palaeo-ELAs indicates the former presence of extensive glaciers; (ii) the presence of peaks in landscape hypsometry below palaeo-ELAs reflects limited/no glaciation; while (iii) peaks in landscape hypsometry below palaeo-ELAs, in conjunction with secondary (subordinate) peaks in hypsometry close to palaeo-ELAs reflects marginal/intermediate glaciation. This scheme focuses upon regions where former glacier cover ranges from 'limited' to 'extensive' and is not applicable to the Sredinny Mountains because the entire area experienced 'full glaciation' at least once during the last glacial cycle (see Barr and Clark, 2012b). However, it can be evolved into a new interpretative scheme where, in fully glaciated regions such as the Sredinny Mountains, the relationship between hypsometric maxima and former ELAs reflects variations in palaeoglacier dynamics (i.e., total ice-flux). In particular, we suggest that in regions where hypsometric maxima and palaeo-ELAs coincide (i.e., where the classic buzzsaw signature is apparent) the ELA effectively acted as a local base level for erosion that was largely limited to areas at or above this altitude (see Egholm et al., 2009) (see Fig. 6A). This is the signature characteristic of the southern sector of the Sredinny Mountains. By contrast, where former glaciers were highly dynamic, they have eroded below their ELAs to excavate deep, flat-bottomed valleys, which in the modern landscape are characterized by

hypsometric distributions skewed toward lower altitudes (see Fig. 5E-F, and Fig. 6B). Based upon this reasoning, highly dynamic glaciers are considered to have occupied the northern sector of the Sredinny Mountains where ice-flux was likely accelerated partly because of high snow accumulation rates in response to moisture availability from the North Pacific, but also because glaciers likely extended offshore and lost mass as they calved into the North Pacific. This combination of increased accumulation and ablation likely sustained high ice-mass flux through the basins (without lowering ELA). In such circumstances, maximum erosion is likely to occur below the ELA because glaciers evacuate sediments from their beds (flushed-out by meltwater) more efficiently (see Cook and Swift, 2012, and references therein), thus exposing the underlying bedrock to erosion. By contrast, basins in the southern sector of the Sredinny Mountains may have been shaped by the action of less dynamic ('typical'), land-terminating glaciers (as in Fig. 1B.) exposed to less favourable climatic conditions in a rain shadow imposed by the Vostočny Mountains to the south and east (see Fig. 1) (a notion supported by Barr and Clark, 2011). Such glaciers were likely less efficient at removing eroded subglacial sediments, which therefore accumulated as thick basal layers and effectively protected the bed from erosion below the ELA (see Cook and Swift, 2012). This notion, that glaciers in the southern sector of the Sredinny Mountains occupied a rain shadow imposed by the Vostočny Range, is supported by Barr and Clark (2011) who suggested that the east–west precipitation gradient currently evident in this region was likely intensified during former periods of glaciation, as ice masses occupying the Vostočny acted as barriers to the inland advection of moisture from the North Pacific (the dominant source of moisture to the region). Further north, beyond the Vostočny Mountains, this precipitation gradient was likely reduced, allowing moisture advection inland to nourish the region's glaciers (see Barr and Clark, 2011). The notion that former glaciers in the northern sector of the mountains were also marine terminating (at least at times) is supported by the on-shore geomorphological record, with a number of large arcuate moraine sequences found extending to (and likely beyond) the modern coastline (see Barr and Clark, 2012a,b), and by the offshore record of ice-rafted debris in the North Pacific, revealing a Kamchatkan origin for former iceberg discharge events (see Bigg et al., 2008).

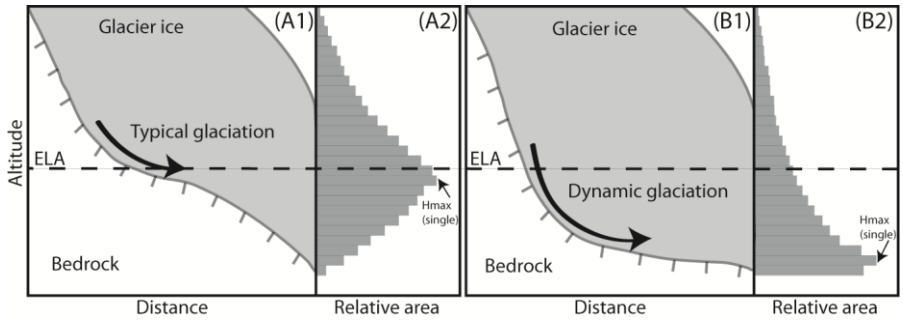

Fig. 6. Schematic illustrations of glacier cross sections and land-surface hypsometric frequency distributions. (A1) Cross section of a 'typical' glacier, which is unable to erode significantly below its ELA. (A2) The land-surface frequency distribution resulting from erosion by the glacier in 'A1'. Here, the ELA has effectively acted as a base level for glacial erosion, resulting in a correspondence between the ELA and the hypsometric maximum ($Hmax_{(single)}$). (B1) Cross section of a dynamic glacier that has eroded a considerable distance below its ELA. (B2) The land-surface frequency distribution resulting from the dynamic glacier in 'B1'. Here, the action of a dynamic glacier has resulted in a low altitude hypsometric maximum ($Hmax_{(single)}$), well below the ELA.

Brocklehurst and Whipple (2006, 2007) found evidence that the tendency for glaciers to erode beneath regional ELAs is a function of basin size, with large glaciers able to incise deeply and incision by smaller glaciers largely restricted to regions above the ELA. Though basin size likely plays a role in governing the degree of glacial erosion, we find little

evidence to suggest that the large-scale trends seen in basin hypsometry in the Sredinny Mountains (as reported in the present study) are related to this factor.

6.3. Where geological forces prevail

In the northern sector of the Sredinny Mountains, the glacial buzzsaw signature is further weakened by the presence of a series of peaks that rise high above the surrounding topography (see Fig. 4 and Table 2). Such peaks have been observed in other glaciated mountain chains and are commonly referred to as 'Teflon peaks' (Anderson, 2005; Foster et al., 2008, 2010; Ward et al., 2012). The principal characteristic of note about these high peaks in the Sredinny Mountains is that, even by the standards of other 'Teflon peaks' (e.g., Foster et al., 2008, 2010), they extend far above the surrounding topography (by as much as 1769 m) and constitute volcanoes either currently 'active' or active during the late Pleistocene and Holocene (Avdeiko et al., 2007; Ponomareva et al., 2007; Bindeman et al., 2010). We also find that these peaks comprise Quaternary Volcanic complexes, surrounded by Miocene–Pliocene complexes (see Fig. 1A), and are therefore comparatively young (Avdeiko et al., 2007). Direct estimates of uplift rates for these Miocene and Quaternary complexes are not available, but we find evidence to suggest 'volcanic construction' during the late Pleistocene and Holocene (see Table 2). However, it is unclear whether the extension of 'Teflon peaks' (numbered in Fig. 4) above the surrounding topography reflects their construction prior to glaciation, during full glacial conditions, following deglaciation (i.e., during the Holocene), or a combination of the above. In fact, in such regions (even without volcanic construction) the action of dynamic glaciers (see section 6.2.1) may well have enhanced the topographic relief of individual high altitude peaks as steep slopes are unable to support large glaciers and instead serve as a source of snow and ice (through avalanching) to low-altitude valley glaciers below (Anderson, 2005; Foster et al., 2010; Ward et al., 2012). This is likely to result in a situation where dynamic glaciers, with high mass-flux, occupy and erode lowland valleys; whilst volcanic peaks remain comparatively ice-free. In this way, topographic relief is enhanced, partly through glacial erosion and partly through flexural isostasy (see Foster et al., 2010; Ward et al., 2012).

7. Conclusions

Topography (peak altitudes), hypsometry, geology, and former ELAs clearly indicate that the height of the Sredinny Mountains has been controlled by the action of a glacial buzzsaw. However, the spatial variability of some of the key parameters considered in this paper has led to the conclusion that a balance between topographic construction and erosion is not always maintained, and we find circumstances where one or the other prevails, or where both act to weaken the glacial buzzsaw signature. In particular:

- In mountain basins characterized by exceptional topographic construction, related to recent volcanism, the glacial buzzsaw signature is seriously weakened by the presence of multiple 'Teflon peaks', such as in the northern sector of the Kamchatkan Sredinny Mountains.
- Mountain basins characterized by favourable climatic and glacial conditions, such as the high precipitation associated with marine-terminating glaciers of the northern Sredinny Mountains, can be occupied by particularly dynamic (high ice-flux) glaciers that can concentrate erosion far below their ELAs, contrary to the notion classically associated with the buzzsaw theory.
- The glacial buzzsaw signature is weakest in mountain basins that experience both volcanic construction and climatic conditions favouring dynamic glaciation, partly

because the latter is enhanced by the accumulation of snow and ice avalanching from the local high altitude 'Teflon peaks'.

Acknowledgements
We thank Simon Brocklehurst, an anonymous reviewer, and the editor, Richard Marston, for their helpful corrections, comments and suggestions.

References

Amundson, J.M., Iverson, N.R., 2006. Testing a glacial erosion rule using hang heights of hanging valleys, Jasper National Park, Alberta, Canada. Journal of Geophysical Research 111, F01020.

Anders, A.M., Mitchell, S.G., Tomkin, J.H., 2010. Cirques, peaks, and precipitation patterns in the Swiss Alps: connections among climate, glacial erosion, and topography. Geology 38 (3), 239-242.

Anderson, R.S., 2005. Teflon peaks: the evolution of high local relief in glaciated mountain ranges. AGU Fall Meeting Abstracts 1 (4).

Anderson, R.S., Molnar, P., Kessler, M.A., 2006. Features of glacial valley profiles simply explained. Journal of Geophysical Research: Earth Surface 111, F01004.

Avdeiko, G.P., Savelyev, D.P., Palueva, A.A., Popruzhenko, S.V., 2007. Evolution of the Kurile-Kamchatkan volcanic arcs and dynamics of the Kamchatka-Aleutian junction. Geophysical Monograph Series – American Geophysical Union 172, 37-55.

Barr, I.D., Clark, C.D., 2011. Glaciers and climate in Pacific far NE Russia during the Last Glacial Maximum. Journal of Quaternary Science 26 (2), 227-237.

Barr, I.D., Clark, C.D., 2012a. An updated moraine map of far NE Russia. Journal of Maps, 8 (3), 1-6.
Barr, I.D., Clark, C.D., 2012b. Late Quaternary glaciations in far NE Russia; combining moraines, topography and chronology to assess regional and global glaciation synchrony. Quaternary Science Reviews 53, 72-87.

Barr, I.D., Spagnolo, M., 2013. Palaeoglacial and palaeoclimatic conditions in the NW Pacific, as revealed by a morphometric analysis of cirques upon the Kamchatka Peninsula. Geomorphology 192, 15-29.

Benn, D.I., Gemmell, A.M.D., 1997. Calculating equilibrium-line altitudes of former glaciers by the balance ratio method: a new computer spreadsheet. Glacial Geology and Geomorphology, http://ggg.qub.ac.uk/papers/full/1997/tn011997/tn01.html.

Bigg, G.R., Clark, C.D., Hughes, A.L.C., 2008. A last glacial ice sheet on the Pacific Russian coast and catastrophic change arising from coupled ice–volcanic interaction. Earth and Planetary Science Letters 265 (3), 559-570.

Bindeman, I.N., Leonov, V.L., Izbekov, P.E., Ponomareva, V.V., Watts, K.E., Shipley, N., Perepelov, A.B., Bazanova, L.I., Jicha, B.R., Singer, B.S., Schmitt, A.K., Portnyagin, M.V.,

Chen, C.H., 2010. Large-volume silicic volcanism in Kamchatka: Ar–Ar and U–Pb ages, isotopic, and geochemical characteristics of major pre-Holocene caldera-forming eruptions. Journal of Volcanology and Geothermal Research 189 (1), 57-80.

Bookhagen, B., Strecker, M.R., 2008. Orographic barriers, high-resolution TRMM rainfall, and relief variations along the eastern Andes. Geophysical Research Letters 35, L06403.

Boulton, G.S., 1996. Theory of glacial erosion, transport and deposition as a consequence of subglacial sediment deformation. Journal of Glaciology 42, 43-62.

Brocklehurst, S.H., Whipple, K.X., 2002. Glacial erosion and relief production in the Eastern Sierra Nevada, California. Geomorphology 42, 1-24.

Brocklehurst, S.H., Whipple, K.X., 2004. Hypsometry of glaciated landscapes. Earth Surface Processes and Landforms 29 (7), 907-926.

Brocklehurst, S.H., Whipple, K.X., 2006. Assessing the relative efficiency of fluvial and glacial erosion through simulation of fluvial landscapes. Geomorphology 75 (3), 283-299.

Brocklehurst, S.H., Whipple, K.X., 2007. Response of glacial landscapes to spatial variations in rock uplift rate. Journal of Geophysical Research 112, F02035.

Brozović, N., Burbank, D.W., Meigs, A.J., 1997. Climatic limits on landscape development in the northwestern Himalaya. Science 276 (5312), 571-574.

Cheng, K.Y., Hung, J.H., Chang, H.C., Tsai, H., Sung, Q.C., 2012. Scale independence of basin hypsometry and steady state topography. Geomorphology 171-172, 1-11.

Cook, S.J., Swift, D.A., 2012. Subglacial basins: their origin and importance in glacial systems and landscapes. Earth-Science Reviews 115, 332-372.

Cowton, T., Nienow, P., Bartholomew, I., Sole, A., Mair, D., 2012. Rapid erosion beneath the Greenland ice sheet. Geology 40 (4), 343-346.

Egholm, D.L., Nielsen, S.B., Pedersen, V.K., Lesemann, J.E., 2009. Glacial effects limiting mountain height. Nature 460, 884-887.

Fedotov, S.A., Zolotarskaya, S.B., Maguskin, M.A., Nikitenko, Y.P., Sharoglazova, G.A., 1988. The study of deformations of the earth's surface on the Kamchatka Peninsula: repeated geodetic measurements. Journal of Geodynamics 10 (2), 175-188.

Foster, D., Brocklehurst, S.H., Gawthorpe, R.L., 2008. Small valley glaciers and the effectiveness of the glacial buzzsaw in the northern Basin and Range, USA. Geomorphology 102, 624-639.

Foster, D., Brocklehurst, S.H., Gawthorpe, R.L., 2010. Glacial-topographic interactions in the Teton Range, Wyoming. Journal of Geophysical Research 115, F01007.

Galewsky, J., 2009. Rain shadow development during the growth of mountain ranges: an atmospheric dynamics perspective. Journal of Geophysical Research 114, F01018.

Hallet, B., Hunter, L., Bogen, J., 1996. Rates of erosion and sediment evacuation by glaciers: a review of field data and their implications. Global and Planetary Change 12 (1), 213-235.

Harbor, J.M., Hallet, B., Raymond, C.F., 1988. A numerical model of landform development by glacial erosion. Nature 333, 347-349.

Hourigan, J.K., Solov'ev, A.V., Ledneva, G.V., Garver, J.I., Brandon, M.T., Reiners, P.W., 2004. Timing of syenite intrusions on the eastern slope of the Sredinnyi Range, Kamchatka: rate of accretionary structure exhumation. Geochemistry International 42 (2), 97-105.

Humphrey, N.F., Raymond, C.F., 1994. Hydrology, erosion and sediment production in a surging glacier: Variegated Glacier, Alaska, 1982-83. Journal of Glaciology 40 (136), 539-552.

Krabbendam, M., Glasser, N. F., 2011. Glacial erosion and bedrock properties in NW Scotland: Abrasion and plucking, hardness and joint spacing. Geomorphology 130 (3), 374-383.

MacGregor, K.R., Anderson, R.S., Anderson, S.P., Waddington, E.D., 2000. Numerical simulations of glacial-valley longitudinal profile evolution. Geology 28 (11), 1031-1034.

Mitchell, S.G., Montgomery, D.R., 2006. Influence of a glacial buzzsaw on the height and morphology of the Cascade Range in central Washington State, USA. Quaternary Research 65 (1), 96-107.

Montgomery, D.R., Balco, G., Willett, S.D., 2001. Climate, tectonics, and the morphology of the Andes. Geology 29 (7), 579-582.

Nürnberg, D., Dethleff, D., Tiedemann, R., Kaiser, A., Gorbarenko, S.A., 2011. Okhotsk Sea ice coverage and Kamchatka glaciation over the last 350ka—Evidence from ice-rafted debris and planktonic $\delta^{18}O$. Palaeogeography, Palaeoclimatology, Palaeoecology 310 (3), 191-205.

Ohmura, A., Kasser, P., Funk, M., 1992. Climate at the equilibrium line of glaciers. Journal of Glaciology 38 (130), 397-411.

Oskin, M., Burbank, D.W., 2005. Alpine landscape evolution dominated by cirque retreat. Geology 33 (12), 933-936.

Pedersen, V.K., Egholm, D.L., Nielsen, S.B., 2010. Alpine glacial topography and the rate of rock column uplift: a global perspective. Geomorphology 122, 129-139.

Pérez-Peña, J.V., Azañón, J.M., Azor, A., 2009. CalHypso: An ArcGIS extension to calculate hypsometric curves and their statistical moments. Applications to drainage basin analysis in SE Spain. Computers & Geosciences 35 (6), 1214-1223.

Persits, F.M., Ulmishek, G.F., Steinshouer, D.W., 1997. Maps Showing Geology, Oil and Gas Fields and Geologic Provinces of the Former Soviet Union. Open-File Report 97-470E, U.S. Geological Survey, Denver, Colorado.

Ponomareva, V., Churikova, T., Melekestsev, I., Braitseva, O., Pevzner, M., Sulerzhitsky, L., 2007. Late Pleistocene-Holocene volcanism on the Kamchatka Peninsula, Northwest Pacific region. Geophysical Monograph Series – American Geophysical Union 172, 165-198.

Porter, S.C., 1964. Composite Pleistocene snow line of Olympic Mountains and Cascade Range, Washington. Geological Society of America Bulletin 75 (5), 477-482.

Porter, S.C., 1989. Some geological implications of average Quaternary glacial conditions. Quaternary Research 32 (3), 245-261.

Richmond, G.M., 1965. Glaciation of the Rocky Mountains. In: Wright H.E., Fry, G.D., (Eds.), The Quaternary of the United States. Princeton University Press, Princeton, NJ, pp. 217-230.

Sanders, J.W., Cuffey, K.M., Moore, J.R., MacGregor, K.R., Kavanaugh, J.L., 2012. Periglacial weathering and headwall erosion in cirque glacier bergschrunds. Geology 40 (9), 779-782.

Small, E.E., Anderson, R.S., 1995. Geomorphically driven late Cenozoic rock uplift in the Sierra Nevada, California. Science 270 (5234), 277-280.

Spotila, J.A., Buscher, J.T., Meigs, A.J., Reiners, P.W., 2004. Long-term glacial erosion of active mountain belts: example of the Chugach–St. Elias Range, Alaska. Geology 32 (6), 501-504.

Strahler, A.N., 1952. Hypsometric (area-altitude) analysis of erosional topography. Geological Society of America Bulletin 63 (11), 1117-1142.

Thomson, S.N., Brandon, M.T., Tomkin, J.H., Reiners, P.W., Vásquez, C., Wilson, N.J., 2010. Glaciation as a destructive and constructive control on mountain building. Nature 467 (7313), 313-317.

Tomkin, J.H., Braun, J., 2002. The influence of alpine glaciation on the relief of tectonically active mountain belts. American Journal of Science 302 (3), 169-190.

Walcott, R.C., Summerfield, M.A., 2008. Scale dependence of hypsometric integrals: an analysis of southeast African basins. Geomorphology 96, 174-186.

Ward, D., Anderson, R.S., Haeussler, P.J., 2012. Scaling the Teflon Peaks: rock type and the generation of extreme relief in the glaciated western Alaska Range. Journal of Geophysical Research 117, F01031.

Whipple, K.X., Kirby, E., Brocklehurst, S.H., 1999. Geomorphic limits to climate-induced increases in topographic relief. Nature 401 (6748), 39-43.

Table 1 Statistics for attributes analyzed per basin[a]

Basin	A	$Alt_{(min)}$	$Alt_{(mean)}$	$Alt_{(peak)}$	HI	$Hmax_{(single)}$	$Cirq_{(alt)}$	gLGM ELA
1	257	393	931	1740	0.42	1074	1072	1065
2	120	434	983	1867	0.38	1096	1127	678
3	221	483	1025	1980	0.36	1069	1199	977
4	332	439	1025	1850	0.41	1033	1119	1091
5	135	346	879	1707	0.39	868	1197	1091
6	98	381	949	1657	0.43	997	1054	1082
7	147	298	857	1724	0.39	956	1004	1002
8	107	297	872	1726	0.40	1026	1007	1004
9	285	268	853	1745	0.40	947	1017	1005
10	1115	259	862	2011	0.35	930	1134	1128
11	1124	293	853	1769	0.38	866	1044	989
12	429	264	773	1747	0.35	690	1077	1012
13	913	225	840	1947	0.36	723	1160	1132
14	3848	103	917	2060	0.42	1003	1251	1195
15	150	142	681	1599	0.37	341	-	714
16	176	67	650	1722	0.35	255	1087	813
17	182	67	713	1749	0.38	712	1115	819
18	462	29	653	1729	0.37	100	1110	1108
19	541	19	652	1836	0.36	405	1024	893
20	458	20	666	2492	0.26	433	1106	925
21	419	3	576	2507	0.22	372	1085	730
22	694	6	595	2596	0.23	250	1090	861
23	621	0	470	1634	0.28	168	879	810
24	1080	40	518	1457	0.33	177	724	852
25	1353	52	568	2124	0.25	350	913	866
26	768	104	626	2200	0.25	294	910	868
27	180	338	865	1787	0.36	909	1062	899
28	768	136	521	2185	0.19	284	868	862
29	1141	84	451	1778	0.21	218	1021	818
30	1053	10	518	1949	0.26	377	1040	754
31	1300	22	606	2626	0.22	81	754	749
32	2078	3	461	2175	0.22	143	730	729
33	1306	3	570	2130	0.27	30	708	705
34	628	7	474	1489	0.32	32	698	691
35	1089	3	495	1539	0.33	66	789	780
36	405	19	408	1304	0.29	122	575	775
37	338	14	304	1122	0.26	66	596	768
38	1684	2	441	1733	0.26	26	831	759
39	927	2	343	1354	0.26	18	715	612
40	492	7	391	1232	0.31	60	660	624
41	509	2	275	1153	0.25	103	680	670
42	277	38	369	1063	0.31	273	-	741
43	128	347	857	1586	0.43	957	966	854
44	176	296	891	1728	0.41	1074	1087	921
45	642	257	934	2104	0.39	909	1273	1080
46	589	193	922	2002	0.41	998	1197	1059
47	398	175	756	1926	0.33	1022	-	697
48	578	273	856	1827	0.37	951	1107	937
49	238	431	860	1754	0.34	569	1110	813
50	180	499	980	1860	0.34	595	1177	826
51	287	393	1007	3621	0.19	511	997	889
52	655	226	654	1931	0.25	673	994	991
53	620	264	753	1806	0.31	490	1024	954
54	1635	210	828	1982	0.35	897	1138	1037
55	2799	219	872	1988	0.37	779	1087	1085
56	1374	323	914	2010	0.36	774	1236	1084
57	2728	223	888	3409	0.21	795	1130	1130
58	2999	237	896	3601	0.20	960	1167	884
59	1737	330	768	1888	0.28	743	978	987
60	2346	190	785	2495	0.23	786	1163	956
61	1324	148	539	2453	0.18	351	978	937
62	2480	68	538	2340	0.20	233	1003	821
63	943	121	685	2417	0.26	323	1312	763
64	779	126	592	1984	0.24	282	1138	926
65	841	129	665	2174	0.25	252	999	764
66	1379	93	602	2620	0.21	219	866	862
67	690	122	597	2449	0.20	355	870	876
68	1996	28	562	2098	0.24	359	903	889
69	1611	56	563	1740	0.27	293	867	865
70	1624	84	646	1855	0.31	521	932	958
71	1159	134	706	1804	0.34	558	1114	816
72	1791	80	650	1829	0.33	467	1035	841
73	384	183	480	1212	0.28	387	-	798
74	599	151	864	1856	0.41	998	1020	969
75	276	237	780	1749	0.33	788	971	896
76	938	50	564	1547	0.32	474	811	800
77	110	247	550	1205	0.31	294	699	682
78	45	248	619	1516	0.28	570	895	821
79	184	206	568	1433	0.30	316	886	780
80	80	250	597	1224	0.35	372	684	788
Min	45	0	275	1063	0.18	18	575	612

Mean	869	170	691	1910	0.31	535	987	884
Max	3848	499	1025	3621	0.43	1096	1312	1195

[a]A, area (km^2); $Alt_{(min)}$, $Alt_{(mean)}$, $Alt_{(peak)}$, minimum, mean, maximum altitude (m asl); HI, hypsometric integral; $Hmax_{(single)}$, single most prominent hypsometric maximum (m asl); $Cirq_{(alt)}$, minimum altitude of cirques (m asl); gLGM ELA, equilibrium-line altitude at the global Last Glacial Maximum (gLGM)(m asl).

Table 2 Details of peaks within the Sredinny Mountains extending more than 500 m above the peak altitude regression line in Fig. 4.

Peak ID[a]	Peak name	Latitude (° N.)	Longitude (° E.)	Altitude	Altitude above regression line	Description
1	Ichinsky volcano	55.68	157.73	3621	1769	Late Pleistocene-Holocene stratovolcano (Ponomareva et al., 2007). Last dated eruption: A.D. 740 (Ponomareva et al., 2007). Currently classed as 'active' (Avdeiko et al., 2007; Bindeman et al., 2010).
2	Alney-Chashakondzha volcanic complex	56.70	159.65	2598	740	Pleistocene volcanic massif with a Holocene eruptive centre (Ponomareva et al., 2007). Last dated eruption < 350 ^{14}C yBP (Ponomareva et al., 2007). Currently classed as 'extinct' (Avdeiko et al., 2007).
3	Shishel volcano	57.45	160.37	2525	606	Shield volcano, active during the Holocene and Late Pleistocene (Bindeman et al., 2010). Currently classed as 'extinct' (Avdeiko et al., 2007).
4	Khuvkhoitun volcano	57.92	160.67	2616	866	Stratovolcano, likely active during the Holocene and late Pleistocene (Ponomareva et al., 2007; Bindeman et al., 2010). Currently classed as 'extinct' (Avdeiko et al., 2007).
5	Ostry volcano	58.18	160.82	2552	830	Stratovolcano, active during the Holocene and late Pleistocene (Bindeman et al., 2010). Last dated eruption ~ 4000 ^{14}C yBP, based upon X Cone (Ponomareva et al., 2007). Currently classed as 'extinct' (Avdeiko et al., 2007).

[a]This is the ID used in Figs. 1 and 4.

Table 3 Pearson product moment correlation among analysed attributes[a]

	A	$Alt_{(min)}$	$Alt_{(mean)}$	$Alt_{(peak)}$	HI	$Hmax_{(single)}$	$Cirq_{(alt)}$	gLGM ELA
A	1.00	-0.30	-0.05	0.45	-0.35	-0.05	0.10	0.26
$Alt_{(min)}$		1.00	0.82	0.07	0.47	0.77	0.48	0.45
$Alt_{(mean)}$			1.00	0.35	0.57	0.89	0.74	0.69
$Alt_{(peak)}$				1.00	-0.49	0.16	0.41	0.27
HI					1.00	0.62	0.31	0.40
$Hmax_{(single)}$						1.00	0.66	0.63
$Cirq_{(alt)}$							1.00	0.65
gLGM ELA								1.00

[a]See Table 1 for definition of attributes.